

Facet-Selective 2D Self-Assembly of TiO₂ Nanoleaves via Supramolecular Interactions

Cheng Yang,[†] Zhimou Yang,[†] Hongwei Gu,[†] Chris K. Chang,^{*,†} Ping Gao,[‡] and Bing Xu^{*,†}

Department of Chemistry and Department of Chemical Engineering, The Hong Kong University of Science and Technology, Hong Kong SAR, China

Received August 5, 2008. Revised Manuscript Received October 19, 2008

Using catechol-group-terminated Zn(II)–porphyrin (ZnP) to functionalize the single-crystalline TiO₂ nanoleaves and coordinate ZnP with *trans*-2,2′-ethylene 4, 4′-bipyridyl (**1**), we demonstrate the self-assembly of TiO₂ nanoleaves based on a supramolecular interaction. Compound **1** cross-links the adjacent TiO₂ nanoleaves along the [101] face, results in a facet-selective, self-assembled, 2D stacking structure. This observation suggests that supramolecular interactions offer a promising route to control anisotropic nanomaterials into designed geometry.

Introduction

This article describes the self-assembly of single crystalline TiO₂ nanoleaves into an anisotropic 2D ordered nanostructure via dative coordination bonds. The use of coordination bonds has led to the construction of sophisticated supramolecular architecture or materials in a range of dimensions.^{1–9} Glotzer and Solomon gave a lot of examples of the anisotropic building blocks of the nanosized particles and colloids.¹⁰ Recently, Fujita et al. further expanded the scope of supramolecular architectures (e.g., macrocycles, ribbons, and cages^{11,12}) based on metal coordination bonds. Using the classical metal–carbon bonds, Stang et al. investigated the self-assembly property of discrete cyclic nanostructures mediated by transition metals.^{1,13,14} Zn(II) porphyrin–ligand supramolecular interaction has been used in several works in recent years, which showed excellent self-assembly efficiency and may result in potential applications because porphyrins have exhibited potentials to serve as components

of nanoscale photonic devices and materials.^{9,15–22} For instance, several groups have reported studies on porphyrin-functionalized carbon nanotubes,^{23,24} gold electrode,^{25–27} gold clusters, nanoparticles,^{26,27} and heterodimers of nanoparticles.²⁸ These representative works clearly demonstrated the power of metal–ligand interactions and the versatility of porphyrin scaffold for generating supramolecular assemblies and useful nanodevices.

Similarly, the development of nanomaterials also suggests that it is essential for nanomaterials to organize into certain superstructures for useful applications.^{29–34} The exploration of the self-assembly of nanomaterials, however, still remains

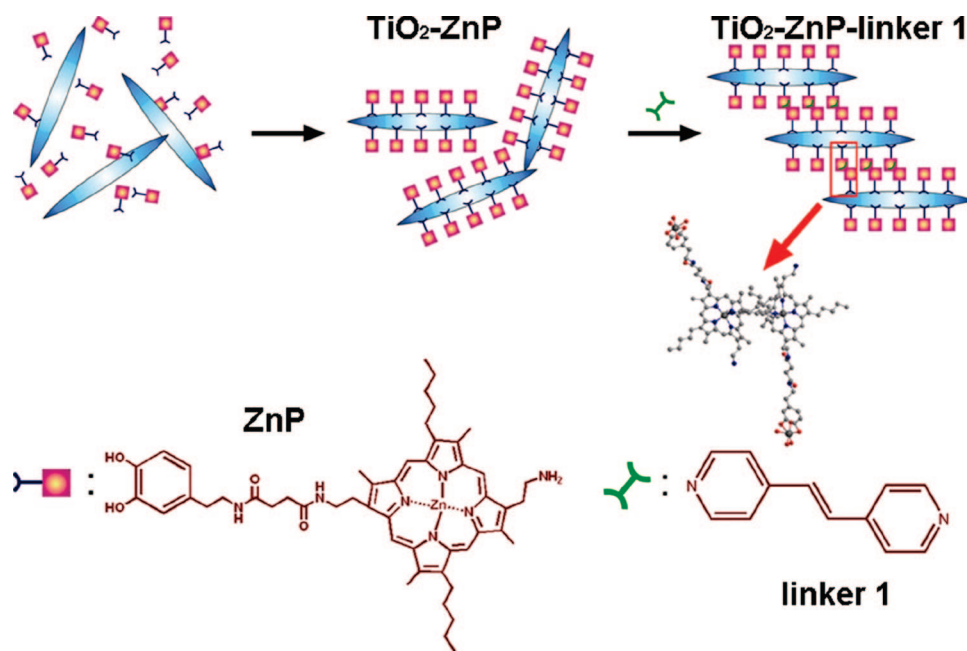
* Corresponding author. E-mails: chang@ust.hk. chbingxu@ust.hk. Tel: 852-2358-7351. Fax: 852-2358-1594

[†] Department of Chemistry, The Hong Kong University of Science and Technology.

[‡] Department of Chemical Engineering, The Hong Kong University of Science and Technology.

- (1) Leininger, S.; Olenyuk, B.; Stang, P. J. *Chem. Rev.* **2000**, *100*, 853.
- (2) Lehn, J. M. *Angew. Chem., Int. Ed.* **1990**, *29*, 1304.
- (3) Holliday, B. J.; Mirkin, C. A. *Angew. Chem., Int. Ed.* **2001**, *40*, 2022.
- (4) Yaghi, O. M.; Li, H.; Davis, C.; Richardson, D.; Groy, T. L. *Acc. Chem. Res.* **1998**, *31*, 474.
- (5) Batten, S. R.; Murray, K. S. *Coord. Chem. Rev.* **2003**, *246*, 103.
- (6) James, S. L. *Chem. Soc. Rev.* **2003**, *32*, 276.
- (7) Fujita, M. *Chem. Soc. Rev.* **1998**, *27*, 417.
- (8) Yaghi, O. M.; O’Keeffe, M.; Ockwig, N. W.; Chae, H. K.; Eddaoudi, M.; Kim, J. *Nature* **2003**, *423*, 705.
- (9) Tsuda, A.; Sakamoto, S.; Yamaguchi, K.; Aida, T. *J. Am. Chem. Soc.* **2003**, *125*, 15722.
- (10) Glotzer, S. C.; Solomon, M. J. *Nat. Mater.* **2007**, *6*, 557.
- (11) Fujita, M.; Umemoto, K.; Yoshizawa, M.; Fujita, N.; Kusakawa, T.; Biradha, K. *Chem. Commun.* **2001**, 509.
- (12) Fujita, M.; Fujita, N.; Ogura, K.; Yamaguchi, K. *Nature* **1999**, *400*, 52.
- (13) Olenyuk, B.; Fechtenkotter, A.; Stang, P. J. *J. Chem. Soc., Dalton Trans.* **1998**, 1707.
- (14) Fan, J.; Whiteford, J. A.; Olenyuk, B.; Levin, M. D.; Stang, P. J.; Fleischer, E. B. *J. Am. Chem. Soc.* **1999**, *121*, 2741.

- (15) Takahashi, R.; Kobuke, Y. *J. Am. Chem. Soc.* **2003**, *125*, 2372.
- (16) Ogawa, K.; Zhang, T. Q.; Yoshihara, K.; Kobuke, Y. *J. Am. Chem. Soc.* **2002**, *124*, 22.
- (17) Kuciauskas, D.; Liddell, P. A.; Lin, S.; Johnson, T. E.; Weghorn, S. J.; Lindsey, J. S.; Moore, A. L.; Moore, T. A.; Gust, D. *J. Am. Chem. Soc.* **1999**, *121*, 8604.
- (18) Slagt, V. F.; Kamer, P. C. J.; van Leeuwen, P.; Reek, J. N. H. *J. Am. Chem. Soc.* **2004**, *126*, 1526.
- (19) Hajjaj, F.; Yoon, Z. S.; Yoon, M. C.; Park, J.; Satake, A.; Kim, D. H.; Kobuke, Y. *J. Am. Chem. Soc.* **2006**, *128*, 4612.
- (20) Wang, Z. C.; M., C. J.; Shelnutt, J. A. *J. Am. Chem. Soc.* **2004**, *126*, 15954.
- (21) Holten, D. B.; D., F.; Lindsey, J. S. *Acc. Chem. Res.* **2002**, *35*, 57.
- (22) Hasobe, T.; Imahori, H.; Fukuzumi, S.; Kamat, P. V. *J. Mater. Chem.* **2003**, *13*, 2515.
- (23) Li, H. P.; Zhou, B.; Lin, Y. G. L. R.; Wang, W.; Fernando, K. A. S.; Kumar, S.; Allard, L. F.; Sun, Y. P. *J. Am. Chem. Soc.* **2004**, *126*, 1014.
- (24) Hasobe, T.; Fukuzumi, S.; Kamat, P. V. *J. Am. Chem. Soc.* **2005**, *127*, 11884.
- (25) Fudickar, W. Z. J.; Ruhlmann, L.; Schneider, J.; Roldner, B.; Siggel, U.; Fuhrhop, J. H. *J. Am. Chem. Soc.* **1999**, *121*, 9539.
- (26) Imhoir, H. F.; S. *Adv. Mater.* **2001**, *13*, 1197.
- (27) Imahori, H. K. Y.; Endo, Y.; Hanada, T.; Nishimura, Y.; Yamazaki, I.; Araki, Y.; Ito, O.; Fukuzumi, S. *Langmuir* **2004**, *20*, 73.
- (28) Gu, H. W.; Xu, K. M.; Yang, Z. M.; Chang, C. K.; Xu, B. *Chem. Commun.* **2005**, 4270.
- (29) Colfen, H.; Mann, S. *Angew. Chem., Int. Ed.* **2003**, *42*, 2350.
- (30) Huynh, W. U.; Dittmer, J. J.; Alivisatos, A. P. *Science* **2002**, *295*, 2425.
- (31) Spatz, J. P. *Angew. Chem., Int. Ed.* **2002**, *41*, 3359.
- (32) Hammond, P. T. *Adv. Mater.* **2004**, *16*, 1271.
- (33) Sarikaya, M.; Tamerler, C.; Jen, A. K. Y.; Schulten, K.; Baneyx, F. *Nat. Mater.* **2003**, *2*, 577.
- (34) Bartl, M. H.; Boettcher, S. W.; Frindell, K. L.; Stucky, G. D. *Acc. Chem. Res.* **2005**, *38*, 263.

Scheme 1. Illustration of Coordination-Bond-Assisted Self-Assembly of TiO₂ Nanoleaves

at its early stage and mainly utilizes isotropic or highly symmetric nanoscale building blocks. For example, nanospheres can self-assemble into hexagonal and cubic arrays, and nanorods into lamellar and nematic arrays.^{35–37} Mann's group assembled the 3D aggregates of gold nanorods using the complimentary DNA linker.³⁸ Rajh et al. reported a self-assembled end-to-end structure of oligomeric TiO₂ nanorods through biotin–avidin cross-linking.³⁹ Grzybowski et al. also reported elegant assembly of nanocrystals via the control of surface chemistry.⁴⁰ There is also an example using van der Waals force to anisotropically control the assembly of gold nanoparticles.⁴¹ Despite these representative examples, there is no report on the self-assembly of anisotropic nanomaterials that possess low symmetry (e.g., nanoleaves or nanoprisms). Among common anisotropic nanomaterials, TiO₂, an important inorganic semiconductor, exhibited various shapes (i.e., rods, leaves, and fibers) on nanoscale.^{39,42–44} Some of the inorganic materials such as metal or metal oxide have been fabricated into TiO₂ nanostructures using sol–gel method or doping method.^{34,45–48} For example, Au, Pt, Ru–RuO_x, and Ir, etc., showed a high affinity to rutile phase TiO₂. The reduced TiO₂ surfaces show stronger binding efficiency than the stoichiometric ones, partially because of the oxygen vacancies.⁴⁹ Because different facets of the TiO₂ nanocrystals have different capabilities for functionalization, self-as-

sembled anisotropic nanostructures would be easier to achieve by using supramolecular interactions that are reversible and reject defects. Despite such a relatively simple principle, there are only few cases that utilize supramolecular chemistry to generate self-assembled structures of TiO₂ nanocrystals.³⁹

Herein, we studied TiO₂ nanoleaves as the building blocks to form self-assembled nanostructures via metal ligand interaction. As shown in Scheme 1, we synthesized and modified the TiO₂ nanoleaves with Zn(II) porphyrin derivative (ZnP)^{49–51} via a general ligand exchange method and used *trans*-2,2'-ethylene-4,4'-bipyridyl (**1**) to interconnect the zinc metal centers of the porphyrin moiety on the [101] face of the TiO₂ nanoleaves.^{52,53} This process afforded a self-assembled nanostructure in a “side-by-side” fashion.^{49,54} The procedure described here generates anisotropic arrays of TiO₂ nanoleaves with controlled distance between crystals and a geometrical arrangement resulting from coordination linkage. This work suggests that metal ligand bonding can act as an element of supramolecular interactions for assisting the self-assembly of the nanomaterials along selected crystal facets to form ordered anisotropic nanostructures, which ultimately

(35) Tian, B. Z.; Liu, X. Y.; Yang, H. F.; Xie, S. H.; Yu, C. Z.; Tu, B.; Zhao, D. Y. *Adv. Mater.* **2003**, *15*, 1370.
 (36) Yang, H. G.; Zeng, H. C. *Chem. Mater.* **2003**, *15*, 3113.
 (37) Bullen, H. A.; Garrett, S. J. *Nano Lett.* **2002**, *2*, 739.
 (38) Dujardin, E.; Hsin, L. B.; Wang, C. R. C.; Mann, S. *Chem. Commun.* **2001**, 1264.
 (39) Dimitrijevic, N. M.; Saponjic, Z. V.; Rabatic, B. M.; Rajh, T. *J. Am. Chem. Soc.* **2005**, *127*, 1344.
 (40) Kalsin, A. M.; Fialkowski, M.; Paszewski, M.; Smoukov, S. K.; Bishop, K. J. M.; Grzybowski, B. A. *Science* **2006**, *312*, 420.
 (41) Zhang, H.; Wang, D. Y. *Angew. Chem., Int. Ed.* **2008**, *47*, 3984.
 (42) Cozzoli, P. D.; Comparelli, R.; Fanizza, E.; Curri, M. L.; Agostiano, A.; Laub, D. J. *Am. Chem. Soc.* **2004**, *126*, 3868.
 (43) Li, D.; Xia, Y. N. *Nano Lett.* **2003**, *3*, 555.
 (44) Wen, P. H.; Itoh, H.; Feng, Q. *Chem. Lett.* **2006**, *35*, 1226.

(45) Akita, T.; Okumura, M.; Tanaka, K.; Tsubota, S.; Haruta, M. *J. Electron. Microsc.* **2003**, *52*, 119.
 (46) Iddir, H.; Skavysh, V.; Ogut, S.; Browning, N. D.; Disko, M. M. *Phys. Rev. B* **2006**, *73*.
 (47) Akita, T.; Lu, P.; Ichikawa, S.; Tanaka, K.; Haruta, M. *Surf. Interface Anal.* **2001**, *31*, 73.
 (48) Ruterana, P.; Buffat, P. A.; Thampi, K. R.; Graetzel, M. *Mater. Res. Soc. Symp. Proc.* **1989**, *139*, 327.
 (49) Ramamoorthy, M.; Vanderbilt, D.; Kingsmith, R. D. *Phys. Rev. B* **1994**, *49*, 16721.
 (50) Diebold, U.; Ruzycski, N.; Herman, G. S.; Selloni, A. *Catal. Today* **2003**, *85*, 93.
 (51) Gong, X. Q.; Selloni, A.; Batzill, M.; Diebold, U. *Nat. Mater.* **2006**, *5*, 665.
 (52) Twyman, L. J.; King, A. S. *Chem. Commun.* **2002**, *8*, 910.
 (53) Lehn, J. M.; Rigault, A.; Siegel, J.; Harrowfield, J.; Chevrier, B.; Moras, D. *Proc. Natl. Acad. Sci. U.S.A.* **1987**, *84*, 2565.
 (54) Rajh, T.; Chen, L. X.; Lukas, K.; Liu, T.; Thurnauer, M. C.; Tiede, D. M. *J. Phys. Chem. B* **2002**, *106*, 10543.

may offer an effective approach to build micro- or mesoscale hierarchical structures from molecular and nanosized building blocks.^{40,55}

Experimental Section

Instrumentation. The absorption spectra of the solution were taken on a Milton Roy 3000 array scan UV-vis spectrophotometer, the excitation spectra of the solution on a Perkin-Elmer S 55 system, and the optical images of the nanocomposites on an Olympus BX41 microscope. The morphologies and sizes of the samples were examined on a JEOL 2010 transmission electron microscope (TEM) with the acceleration voltage of 200 kV, the species and crystallinity of the TiO₂ nanoleaves on a powder X-ray diffractometer_panalytical (XRD), Model X'pert Pro. with CuK α ' radiation generated at 40 kV and 100 mA, in the range of 20° to 60° at a scan speed of 4°/min. The surface energy of the nanocomposites on a Physical Electronics PHI 5600 X-ray photoelectron spectroscopy (XPS), the characterization of the surface composition of the nanocomposites on a Physical Electronics time-of-flight secondary ion mass spectroscopy PHI7200 (ToF-SIMS). The chemical spectra were acquired in the negative mode using a Ga⁺ liquid metal ion source operating at 25 keV. The total ion dose was lower than 4×10^{12} ions/cm² under a high vacuum of 1.5×10^{-9} Torr. A digital instruments scanning probe microscope-nanoscope atomic force microscope (AFM) was used to characterize the surface morphology of TiO₂ nanoleaves.

Synthesis of the Porphyrin Derivatives. The synthetic route of the catechol terminated porphyrin follows an earlier work reported by Gu et al.²⁸ ZnP derivative was prepared by adding 50 mg of zinc acetate into the CH₃OH/CHCl₃ (1:1) solution of the catechol terminated porphyrin (100 mg in 50 mL) and stirring overnight. The excess amount of zinc acetate was filtered on a silica gel column (yield = 61%) (see the Supporting Information).

Synthesis of the TiO₂ Nanoleaves. As in a typical procedure, 1 mL (3.5 mmol) of titanium(IV) isopropoxide and 3 mL (29 mmol) of triethyl amine (NEt₃) were mixed in 76 mL of water by ultrasound to obtain a translucent solution. The solution was sealed in a Teflon-lined stainless steel vessel and cured at 140 °C for 48 h. After centrifuging the aggregated impurities, the white milky product was washed using 10 M HNO₃ and deionized water with ultracentrifuge until the pH value was neutralized. Then the product was collected and dried at 60 °C in vacuum (yield = 78%) to give white powder.

Anchoring Porphyrin on the TiO₂ Surface. 100 mg TiO₂ nanoleaves were dispersed into 5 mL CH₃OH/CHCl₃ (1:1) solution. ZnP (0.1 mg, in 100 μ L of CH₃OH/CHCl₃ = 1:1) was injected into the TiO₂ suspension, which was subsequently sonicated for 3 min. The mixture was stirred at room temperature for 24 h. Afterward, the TiO₂ suspension was purified by centrifugation to remove the excess amount of porphyrin and finally redispersed into 10 mL of the same solvent. A drop of this TiO₂ solution was dropcasted on a carbon-coated TEM copper grid and dried in a vacuum for 8 h.

Cross-Linking of the TiO₂ Nanoleaves. TiO₂ nanoleaves-ZnP was cross-linked and transformed into TiO₂ nanoleaves-ZnP-1 according to the following method: Typically **1** (0.05 mg, in 50 μ L of CH₃OH/CHCl₃ = 1:1) was injected into the TiO₂ nanoleaves-ZnP solution (0.2 g, in 20 mL of CH₃OH/CHCl₃ = 1:1) (according to the concentration of TiO₂ nanoleaves in the solution and the density of TiO₂, there are about 100 molecules of **1** per TiO₂ nanoleaf). The nanocomposite was collected and redispersed in 20

mL of CH₃OH/CHCl₃ = 1:1 and diluted into different concentrations (0.5, 1.5, and 3 mg/mL). Each of the samples was dropcasted on a piece of carbon-coated copper grid and dried in a vacuum for at least 8 h before TEM analysis.

TiO₂ nanoleaves-ZnP-2 and TiO₂ nanoleaves-ZnP-3 were prepared according to the following method: 50 μ L (1 mg/mL) of 4, 4'-bipyridine (**2**) or pyridine (**3**) is injected into 20 mL (10 mg/mL) of TiO₂ nanoleaves-ZnP solution (about 100 molecules of **2** or **3** per TiO₂ nanoleaf according to the concentration of TiO₂ nanoleaves in the solution). The nanocomposite was collected and redispersed in 20 mL CH₃OH/CHCl₃ (1:1) solution and diluted into different concentrations (0.5, 1.5, and 3 mg/mL). A drop of each of the solutions was then dropcasted on carbon-coated copper grid and dried in a vacuum for at least 8 h before TEM analysis.

Results and Discussion

Morphological Characterization of the TiO₂ Nanoleaves. The pristine TiO₂ nanoleaves were examined on TEM, AFM, and XRD. The TEM observations revealed that the TiO₂ products consisted of regular, straight, and smooth crystalline nanoleaves that were randomly scattered on the carbon film. A careful measurement of the TiO₂ nanoleaves in a TEM picture showed that the average length and width of the TiO₂ nanoleaves were $\sim 201 \pm 36$ nm and $\sim 25 \pm 5$ nm, respectively, which afforded a typical aspect ratio of about 8. Through AFM analysis, we further observed the topology of the nanoleaves. From the AFM image, the thickness-to-width ratio in the middle part of the nanoleaf was ~ 3.7 , showing a flat leaf-like structure. The selected area electron diffraction (SAED) patterns confirmed the high crystallinity of the nanoleaves, whose diffraction patterns matched the crystal planes of anatase TiO₂. The high-resolution TEM further confirmed the good crystallinity of those anatase TiO₂ nanoleaves.

UV/FL Spectra & Optical/FL Images. The solid state UV-vis spectra of the TiO₂-porphyrin samples are shown in Figure 1a as strong Soret bands and weak Q bands. Upon the adsorption of the porphyrin molecules on nanocrystalline TiO₂ surface, not only the Q bands are red-shifted and broaden but a weak absorption feature appears on the red side of the solution-like Soret bands at 418 nm, which reflects a large proportion of monomeric porphyrin adsorbed on TiO₂ nanoleaf surfaces. This reveals a weak interaction between porphyrin and TiO₂ nanoleaves. The appearance of the red-shift (Figure 1a, A \rightarrow B) is attributed to the aggregation of porphyrin assemblies on the surfaces of the TiO₂ caused by the J-aggregation of porphyrins on the TiO₂ surfaces. Fluorescence emission at 596 nm (Figure 1b, A \rightarrow B) is quenched by J-type aggregation. The H-aggregation of the ZnP on the TiO₂ surfaces generates a blue-shift of the absorbance in Figure 1b, B \rightarrow C.⁵⁶ When **1** is added, the absorption exhibits a red shift from 402 to 418 nm in Figure 1a, C \rightarrow D. This demonstrates the electron transfer (ET) process through the conjugated linker **1** between the couple of the Zn-porphyrin center. However, in the fluorescence spectra (C and D in Figure 1b), the electron transfer process was not exhibited because the process happens in nanosecond

(55) Whitesides, G. M.; Grzybowski, B. *Science* **2002**, 295, 2418.

(56) Maiti, N. C.; Mazumdar, S.; Periasamy, N. *J. Phys. Chem. B* **1998**, 102, 1528.

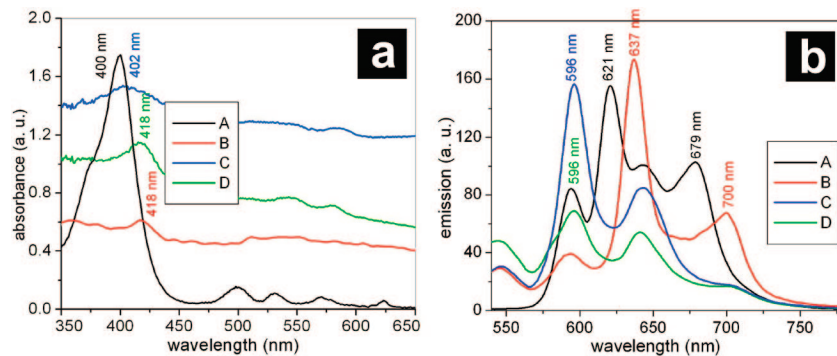


Figure 1. (a) UV-vis absorption spectra of (A) 0.02 mM porphyrin in THF; (B) solid sample of TiO₂ nanoleaves surface grafted with porphyrin; (C) solid sample of TiO₂ nanoleaves surface grafted with ZnP (TiO₂-ZnP); (D) solid sample of TiO₂ nanoleaves with surface cross-linked by ZnP-1. (All the solid samples were measured using reflective mode UV-vis spectroscopy) (b) Fluorescent emissions of (A) porphyrin; (B) TiO₂ nanoleaves surface grafted with porphyrin; (C) TiO₂ nanoleaves surface grafted with ZnP (TiO₂-ZnP); (D) TiO₂ nanoleaves with surface cross-linked by ZnP-1. (Excitation wavelength is 400 nm.)

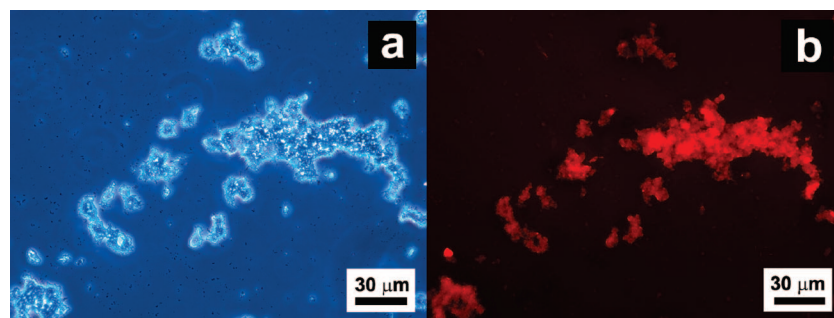


Figure 2. Optical microscopic images of the TiO₂-porphyrin sample: (a) phase image, (b) fluorescence image. The TiO₂ nanoleaves and TiO₂-porphyrin were washed with chloroform 5 times and then observed using an Olympus BX41 microscope. The fluorescence excitation wavelength ranges from 545 to 580 nm, and the emission wavelength ranges from 610 nm to infrared.

time.⁵⁶ We took both phase image and fluorescent image of TiO₂-porphyrin under optical microscope. The bright-red fluorescent image of TiO₂-porphyrin further demonstrated the existence of porphyrin on the surface of TiO₂ nanoleaves (Figure 2). ToF-SIMS analysis on TiO₂-porphyrin showed the characteristic peak of *m/z* 169.0, which indicated the existence of the bonding between the catechol group on the porphyrin moiety and Ti (see the Supporting Information).⁵³ XPS was used to distinguish the binding energy of TiO₂ upon anchoring. Compared to the bare TiO₂ nanoleaves, the peak that was attributed to TiO₂ shifted to higher binding energies by 0.5 eV upon the adsorption of ZnP (see the Supporting Information). These data suggest a substantial interaction between ZnP and the surface of TiO₂ nanoleaves.⁵³

Morphological Analysis. We analyzed TiO₂-ZnP-1 at different concentrations (0.5, 1.5, and 3 mg/mL) using TEM. The concentration of the nanocomposite in the solution for TEM analysis is significant for the observation of the self-assembly structure. These concentrations were selected because most of the nanocomposites can form a monolayer at the carbon film after a natural evaporation of the solvent at room temperature. Higher concentration (e.g., 10 mg/mL) can result in the uncontrolled stacking of the nanocompositions on the carbon film due to the van der Waals force. The morphology of the assemblies of the TiO₂ nanoleaves is illustrated in Figure 3. TiO₂-ZnP-1 solutions with different concentrations were dropped onto copper grid. After the samples were dried at room temperature, all of the samples with three concentrations were analyzed. It is known

that the [101] face is the highest under-coordinated (5-fold coordination) surface of the anatase phase TiO₂ (5.16×10^{14} sites/cm²).⁵⁷ This face has strong affinity to the enediol ligands, which restores the Ti atoms to the octahedral coordination and can form irreversible ligand-to-nanoleaf complexes.⁵⁴ The distance of the adjacent TiO₂ nanoleaves in Figure 3a was measured with Gatan DigitalMicrograph. The adjacent nanoleaves had a regular distance of about 3 nm on the opposing [101] facet. This observation suggests that the [101] facet of the adjacent TiO₂ nanoleaves are interconnected by the porphyrin pairs. Close analysis of the HRTEM image of two pieces of adjacent TiO₂ leaves showed that the closest distance is about 3 nm (Figure 4). The anisotropic arrangement of the nanoleaves suggests that the [101] facet has a preferential bonding potential to the porphyrin derivative compared with the other crystal facets on the TiO₂ nanoleaves. From Figure 3, we can observe that at each concentration of the composite, there was no significant difference in the arrangement of the nanoarrays.

To analyze the effect of **1** and evaluate different pyridyl ligands, we used 4,4'-bipyridine (**2**) (Figure 5) and pyridine (**3**) (Figure 6) as the ligands to coordinate with TiO₂-ZnP for comparison. Because one pyridine (**3**) molecule can only bond with one Zn(II)-porphyrin moiety, it has no cross-linking function for the Zn(II)-porphyrin. 4,4'-bipyridine (**2**) is a rigid linear molecule shorter in length than *trans*-2,2'-

(57) Diebold, U.; Ruzycski, N.; Herman, G. S.; Selloni, A. *Catal. Today* **2003**, *85*, 93.

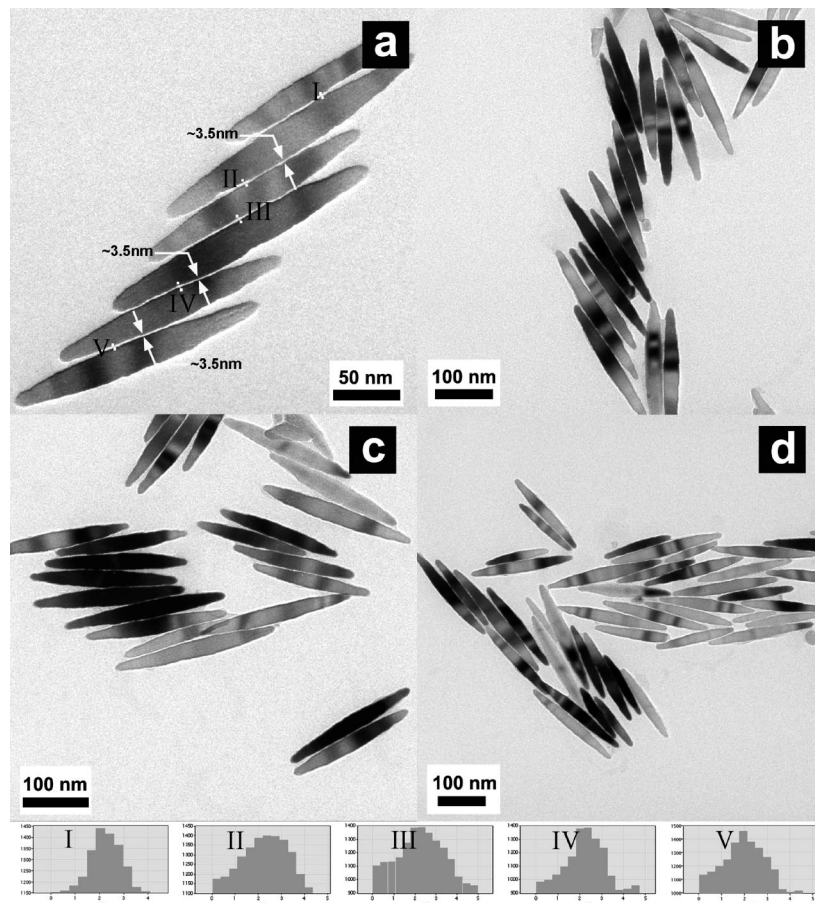


Figure 3. TiO_2 nanoleaves cross-linked by ZnP-1 at different concentrations: (a, b) 1.5, (c) 0.5, and (d) 3 mg/mL. The lower insets show the distance measurements in (a).

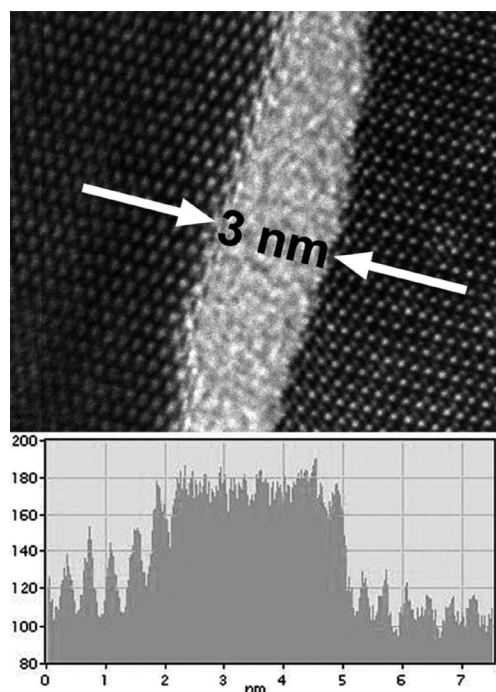


Figure 4. HRTEM image and profile image of two pieces of adjacent TiO_2 nanoleaves and the gap between them (cross-linked by ZnP-1).

ethylene 4,4'-bipyridyl (**1**). Both **1** and **2** have a rigid structure with two pyridine moieties in two ends, which can coordinate with Zn(II)-porphyrin. We characterized TiO_2

nanoleaves modified with the corresponding Zn(II)-porphyrin ligands (TiO_2 -ZnP-2 and TiO_2 -ZnP-3). As shown in Figure 5 and 6, from the TEM observations, TiO_2 -ZnP-2 showed a randomly scattered morphology on copper grids in all the three concentrations for analysis. No organized assembly was found under careful examination. TiO_2 -ZnP-3 was also characterized under TEM, but there was no evidence that this molecule assisted the facet-selected assembly either. In order to compare the binding efficiency of the above ligands, we carried out the UV-vis titration test.⁵³ Table 1 summarizes the binding constants of each ligand. It shows that **2** has weaker binding efficiency to the two metal centers than **1**. This weaker binding may result from the steric effect owing to the shorter length of the molecule of **2**. Ligand **3** (pyridine molecule) does not show a cross-linking function, though the binding constant is higher than **1** and **2**. These control studies suggest that both the length and functionality of the ligand play a key role in the facet-selected assembly of the TiO_2 nanoleaves.

Plausible Explanation and Modeling. By cross-linking the Zn(II)-porphyrin center using **1** at the edge of the TiO_2 nanoleaves, a large proportion of these TiO_2 nanoleaves were self-assembled into anisotropic 2D stacks in nonaqueous media, which could be easily identified under TEM analysis.⁵³ From the TEM observation, the average shortest distance between each adjacent TiO_2 [101] facet is about 3 nm, indicating the axial interconnected double-layer structure of the porphyrin moieties distributed at the surface. Scheme

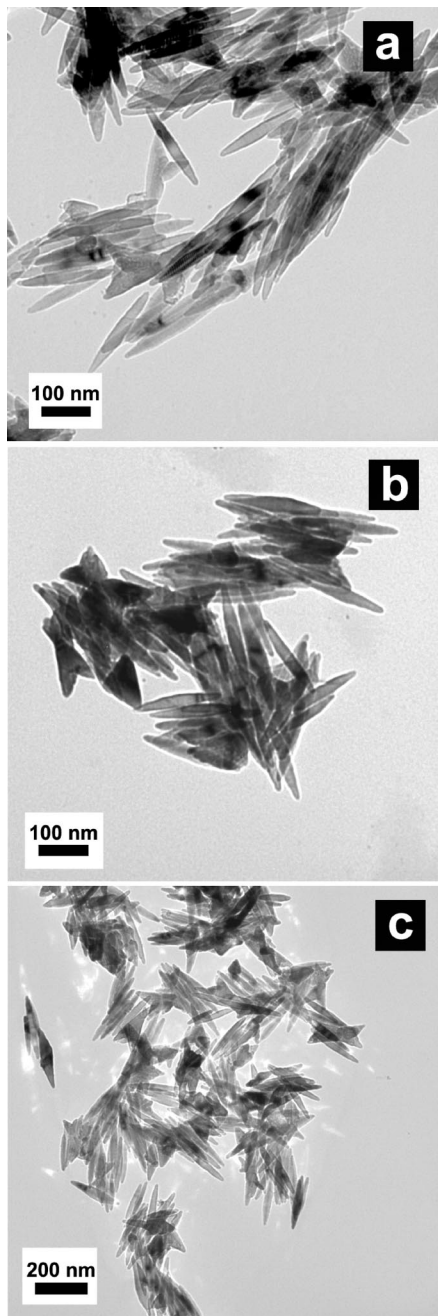


Figure 5. TiO₂ nanoleaves cross-linked by ZnP-2 at different concentrations: (a) 0.5, (b) 1.5, and (c) 3 mg/mL.

2 illustrates the arrangement of the interconnected porphyrin moieties between two opposite TiO₂ [101] facet. According to the computational simulations, we observed that at the lowest energy level, the two [101] facet can have a distance about 2.92 nm; the longest distance between the two ends of the ZnP-1 dimer can not be longer than 5.2 nm (see the Supporting Information). This result matches to the direct TEM observations. Noteworthy, no long-range nanoleaf arrays or large micrometer-sized nanoleaf bundles can be observed. We also noticed that in the TiO₂-ZnP-1 solution, some reddish powder precipitated out after 2–5 h. This means that the TiO₂-ZnP nanocomposites were associated by the ligand and forms larger clusters in the solution. The morphology of the assembly is greatly influenced by the binding efficiency of the ligands. An efficient binding

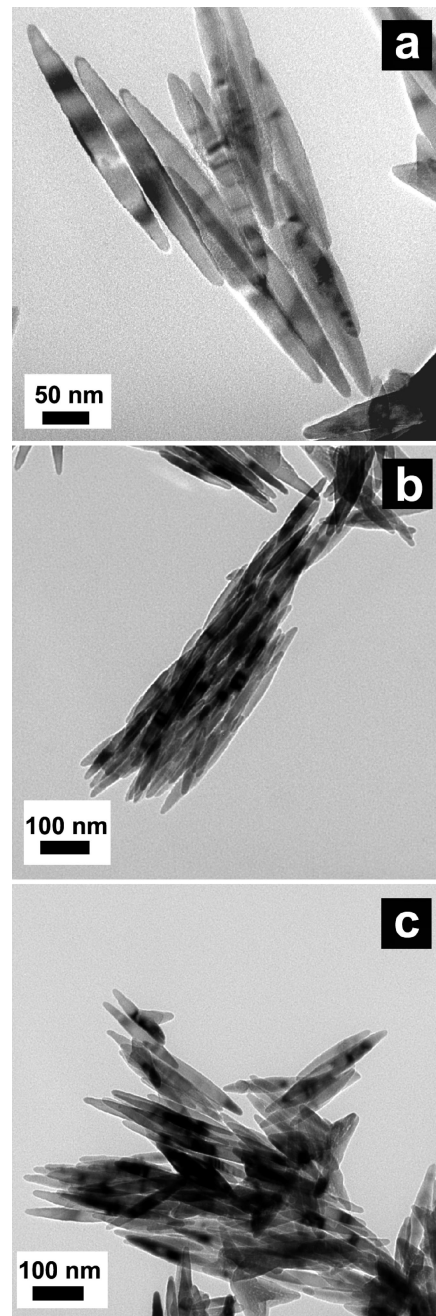
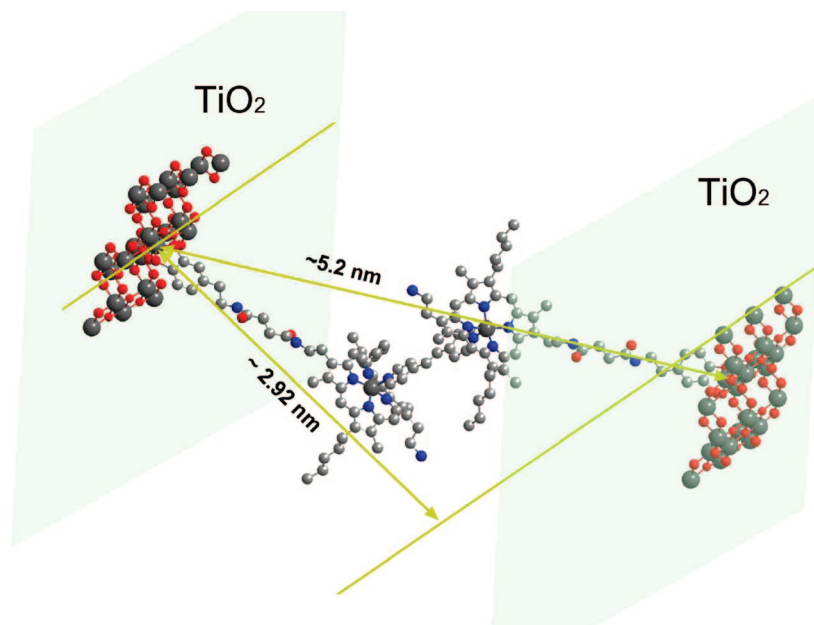


Figure 6. TiO₂ nanoleaves cross-linked by ZnP-3 at different concentrations: (a) 0.5, (b) 1.5, and (c) 3 mg/mL.

Table 1. Binding Constant Test Result of ZnP with Different Pyridine Ligands

	ligand		
	1	2	3
binding constant	$1.55 \times 10^4 \text{ M}^{-1}$	$7.74 \times 10^3 \text{ M}^{-1}$	$1.74 \times 10^5 \text{ M}^{-1}$

between the facet-selected anchored ZnP and the ligand is crucial for building up this assembly. Otherwise, the association of the nanoleaves can not exhibit facet selection behaviors. Considering the other microscopic forces such as van der Waals force and electrostatic force, as the TiO₂ crystalline facet [020] has the largest area, it generates the largest effect in these two kinds of forces than the other facets. Therefore, if any of these two kinds of forces take the predominant responsibility, the “face-to-face” stacking

Scheme 2. Molecular Modeling of ZnP and **1** on the Surface of TiO₂ Nanoleaves

will be the primary phenomenon, just like TiO₂-ZnP-**2** or TiO₂-ZnP-**3** exhibited. According to the UV-vis titration test of the pyridine ligands, we observed that the binding constant of the pyridine moiety on **1** is about two times higher than that on **2** toward ZnP (see the Supporting Information). This makes the **1** cross-linked nanocomposites form the “side-by-side” linkages, rather than the face-to-face stacking on the [101] surface. This phenomenon is obviously different from that of the unmodified nanoleaves (Figure 1a) and the control sample of TiO₂-ZnP-**2**, which did not have the ability to cross-link porphyrins (Figure 5).

The length of the ligand cross-linker is also an important factor to determine the style of the arrangement, as observed in the TEM images in the control experiment. Linker **2** could not induce the well-ordered assemblies of TiO₂ nanoleaves. Under this condition, the TiO₂ nanoleaves only formed randomly aggregated bundles, which suggested that a single molecule of **2** can not bond to the ZnP molecules on two different TiO₂ nanoleaves at the same time.

Conclusions

In summary, we demonstrated that by cross-linking the porphyrin modified TiO₂ nanoleaves via coordination bonds, the TiO₂ nanoleaves can self-assemble into oligomeric anisotropic nanostructure along the [101] facet. These TiO₂ nanoleaves have a 2D stacking morphology and each piece of the TiO₂ nanoleaf is a single crystal. Compared to the previous reports,^{58,59} they showed smaller and more homogeneous morphology. We also further demonstrated that the length of the ligands is an important factor for the assembly efficiency of the TiO₂ nanoleaves. This work suggests an approach to manipulate the TiO₂ self-assembly using Zn(II)-porphyrin and the bidentate bispyridine. Because of

the well-established and diverse chemistry of metal ligand bonds, this work might be useful in designing new types of solar cell with unique current collection or charge transfer properties.^{22,60-72} The photophysical properties of these self-assembled TiO₂ nanoleaves will be the subject of further investigation.

Acknowledgment. This work was partially supported by RGC (Hong Kong). Thanks to Dr. Yu-tao Xie in the Department of Chemistry and Dr. Haibo Fan in the Department of Mechanical Engineering, the Hong Kong University of Science and Technology, for discussions.

Supporting Information Available: Additional images (PDF). This material is available free of charge via the Internet at <http://pubs.acs.org>.

CM8021352

(58) Saponjic, Z. V.; Dimitrijevic, N. M.; Tiede, D. M.; Goshe, A. J.; Zuo, X. B.; Chen, L. X.; Barnard, A. S.; Zapol, P.; Curtiss, L.; Rajh, T. *Adv. Mater.* **2005**, *17*, 965.
 (59) Kanie, K.; Sugimoto, T. *J. Am. Chem. Soc.* **2003**, *125*, 10518.

(60) Jasieniak, J.; Johnston, M.; Waclawik, E. R. *J. Phys. Chem. B* **2004**, *108*, 12962.
 (61) Schmidt-Mende, L.; Campbell, W. M.; Wang, Q.; Jolley, K. W.; Officer, D. L.; Nazeeruddin, M. K.; Gratzel, M. *Chemphyschem* **2005**, *6*, 1253.
 (62) Papageorgiou, N. *Coord. Chem. Rev.* **2004**, *248*, 1421.
 (63) Chappel, S.; Grinis, L.; Ofir, A.; Zaban, A. *J. Phys. Chem. B* **2005**, *109*, 1643.
 (64) Campbell, W. M.; Burrell, A. K.; Officer, D. L.; Jolley, K. W. *Coord. Chem. Rev.* **2004**, *248*, 1363.
 (65) Li, Z. H.; Wang, D. J.; Shi, Y. Y.; Wang, P.; Wang, X. Q. *Mater. Chem. Phys.* **2005**, *90*, 203.
 (66) Nazeeruddin, M. K.; Humphry-Baker, R.; Officer, D. L.; Campbell, W. M.; Burrell, A. K.; Gratzel, M. *Langmuir* **2004**, *20*, 6514.
 (67) Yang, J. H.; Chen, Y. M.; Ren, Y. L.; Bai, Y. B.; Wu, Y.; Jang, Y. S.; Su, Z. M.; Yang, W. S.; Wang, Y. Q.; Zao, B.; Li, T. *J. Photochem. Photobiol. A* **2000**, *134*, 1.
 (68) Wang, Q.; Campbell, W. M.; Bonfantani, E. E.; Jolley, K. W.; Officer, D. L.; Walsh, P. J.; Gordon, K.; Humphry-Baker, R.; Nazeeruddin, M. K.; Gratzel, M. *J. Phys. Chem. B* **2005**, *109*, 15397.
 (69) Kroeze, J. E.; Savenije, T. J.; Warman, J. M. *J. Am. Chem. Soc.* **2004**, *126*, 7608.
 (70) Odobel, F.; Blart, E.; Lagree, M.; Villieras, M.; Boujtita, H.; El Murr, N.; Caramori, S.; Bignozzi, C. A. *J. Mater. Chem.* **2003**, *13*, 502.
 (71) Clifford, J. N.; Yahioglu, G.; Milgrom, L. R.; Durrant, J. R. *Chem. Commun.* **2002**, 1260.
 (72) Kroeze, J. E.; Koehorst, R. B. M.; Savenije, T. J. *Adv. Funct. Mater.* **2004**, *14*, 992.